UNIVERSITI PUTRA MALAYSIA

CHARACTERIZATION OF YTTRIUM BARIUM COPPER OXIDE (YBCO) THIN FILM

NUR FATIHAH BINTI PAWI

CHARACTERIZATION OF YTTRIUM BARIUM COPPER OXIDE (YBCO) THIN FILM

by

NUR FATIHAH BINTI PAWI

196720

A Thesis submitted to
The Department of Physics, Universiti Putra Malaysia
For the degree of
Bachelor of Science in Instrumentation Science with Honours

ABSTRACT

CHARACTERISATION OF YTTRIUM BARIUM COPPER OXIDE (YBCO) THIN FILM

By

NUR FATIHAH BINTI PAWI

January 2022

YBCO thin films are widely known for their potential in achieving higher critical temperature T_c compared to bulk. There are many factors that may affect the superconducting properties of thin films such as the microstructure of the film. This thesis discussed the characterization of YBCO thin film by four methods which are AFM, SEM, EDX and XRD. The microstructure of the samples are investigated as well as the superconducting properties. There were three samples involved which all of them were pure YBCO. The samples exhibits different surface roughness, average grain size and YBCO composition.

ABSTRAK

CIRI-CIRI FILEM NIPIS YTTRIUM BARIUM COPPER OXIDE (YBCO)

Oleh

NUR FATIHAH BINTI PAWI

JANUARI 2022

Filem nipis YBCO terkenal dengan potensinya untuk mencapai suhu kritikal yang lebih tinggi berbanding pukal. Terdapat banyak faktor yang boleh mempengaruhi sifat superkonduktor filem nipis seperti struktur mikro filem. Tesis ini membincangkan pencirian filem nipis YBCO melalui empat kaedah iaitu AFM, SEM, EDX dan XRD. Struktur mikro sampel disiasat serta sifat superkonduktor. Terdapat tiga sampel yang terlibat yang kesemuanya adalah YBCO tulen. Sampel mempamerkan kekasaran permukaan yang berbeza, saiz butiran purata dan komposisi YBCO.

DEDICATION

I dedicated this research to my parents, Pawi bin Senang and Shariah binti Bujang, and all my siblings for giving me support and love throughout my journey in completing this research. Without their love and support, I would not be able to finish my research.

To my supervisor, Assoc. Prof. Dr. Mohd Mustafa bin Awang Kechik, my lecturers and also my peers, Noorshafiyah binti Jamaluddin, Nur Danisha Anum binti Aminuddin, Nur Afiqah binti Mohamed Indera Alim Sah and Farzana Atiqah binti Ahmad Huzaini who have helped me a lot in this research and whenever I am having hard time throughout my learning journey.

Lastly, I devoted myself to my Almighty God for His blessing and guidance along my life. I devoted myself to Him.

TABLE OF CONTENTS

LIST OF FIGURES

LIST OF TABLES

Chapter 1

INTRODUCTION

1.1 Introduction to Superconductor

One of the most intriguing problems in modern solid-state physics is understanding the decades-old mystery of superconductivity at high temperatures, particularly in copper oxide materials. Cuprates, a puzzling class of materials produced from copper oxides, are well-known in the scientific world for having an identity crisis that can cause them to act as both insulators and conductors.

A superconductor is a substance that conducts electricity without resistance. This indicates that when the temperature of the material reaches the critical temperature, T_c for the superconductive state, no energy will be released. The superconductor will conduct electricity effectively before reaching the critical temperature, where this material will turn into a normal metal again. However, the penetration of the magnetic field on the material does not exist during the superconductive state.

By understanding the concept of normal conductivity, the meaning of superconductivity and its unique nature can be comprehended. When electrons, carriers of a negative charge, pass through a material resulting from a force, it is called a conductor of electricity. As voltage is applied to the conductor, the force will be generated by an electric field that is formed. Other than the electric force that is produced from the applied voltage, the magnetic force also plays a significant role in superconductivity.

Researchers have found that moving charges produce magnetic fields and when these electric charges are moving near a magnet, they will experience a force. Magnetic fields act on moving charges, which are then affected on by other magnets, all of which have moving charges (Urone & Hinrichs, 2012). As in superconductors, magnetic fields are expelled from the interior when the electric current is applied to the surface. This phenomenon causes a magnet to levitate above the superconductor. This finding has led to more experiments done by the researchers to explore deeper about superconductors.

1.2 Application of Superconductor

Owing to its unique zero resistivity property, superconductors have wide spread application in various fields of science and technology (Velavan & Myvizhi, 2018). Ever since the discovery of high temperature superconductor, it is much convenient to handle by which it has contributed to multiple technology development including medical field and transportation.

1.2.1 Magnetic Resonance Imaging (MRI)

Magnetic Resonance Imaging (MRI) is a widely used scanner in the medical field either to detect or diagnose diseases and even treatment monitoring. MRI is able to image soft tissue parts in the body and is much safer than x-ray since it does not emit the harmful ionizing radiation as an x-ray does. However, MRI is more expensive compared to x-ray. Because the magnetic resonance spectra of other tissues are different, magnetic resonance imaging is able to differentiate between tissue types such as kidney and liver tissue. (Owens & Poole, 2002).

The main magnet is the key component in MRI system, as shown in Figure 1 because it generates a highly uniform static magnetic field in the region of interest (ROI). The most commonly used magnet is superconductive. This magnet is created comprised of a superconductive coil that is immersed in liquid nitrogen and was cooled with helium liquid in order to make it superconductive. Superconductive magnets produce strong and homogeneous magnetic fields, but they are expensive and require constant maintenance. Furthermore, these magnets are safe for patients since there are safety features such gas evacuation pipes, the capacity to monitor the temperature and oxygen inside the MRI room, and a door that opens outwards to prevent overpressure.

The strength of the magnetic field produced, which is measured in Tesla, is one of the most important characteristics to consider in an MRI system (T). This varies from 0.2 to 3.0 T in contemporary clinical practice. The magnet must be properly calibrated or shimming to obtain the most uniform magnetic field, either passively with movable metal parts or actively with small electromagnetic coils scattered within the magnet. Wang et al., 2020, mentioned that it is difficult to construct a high-performance, low-cost superconducting magnet for MRI applications, especially for those with split MRI configurations, due to the strict engineering limitations of existing superconducting technology.

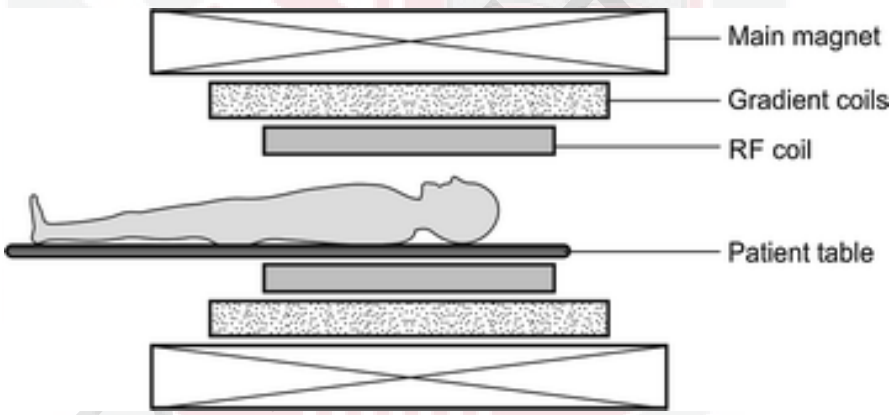

Figure 1. A schematic diagram of a MRI scanner consisting of the main magnet, the gradient coils, the RF coil and the patient table (Sharma, 2015).

1.2.2 Magnetic Levitation Train (MAGLEV)

Automobiles and air services are no longer able to keep up with population growth and the development of urban zones, making mass transit unaffordable. As a result, there has been a rise in demand for new modes of public transportation. A new-generation transportation system must fulfill specific characteristics in order to properly serve the public such as safety of the transport and efficiency. Magnetic levitation trains are one the latest technologies in transportation. Lee et al., 2006, reported that rather than using friction between wheels and rails to propel a train ahead, the Maglev train uses electromagnets to replace wheels and levitates on the guideway, as can be seen in Figure 2 providing propulsion force electromechanically without any contact.

Yaghoubi, 2013 claimed that magnetic levitation is a technique of suspending an object in the air utilizing just magnetic fields as a support. As for magnetic levitation train (MAGLEV), it is an advanced technology which is a frictionless train that operates very efficiently. Since the Maglev train does not make physical touch with its guideway, it has no friction making the train able to move at high speed. Superconducting material and magnetic track are involved in the working of Maglev trains as in Figure 2. Though they haven't been made for a production of commercial use, people have shown that such trains are indeed possible and they carry massive scope for future, as Maglev trains have a very high efficiency because of the fact that the train never touches the track, and the losses due to friction are zero (Kumar, 2019).

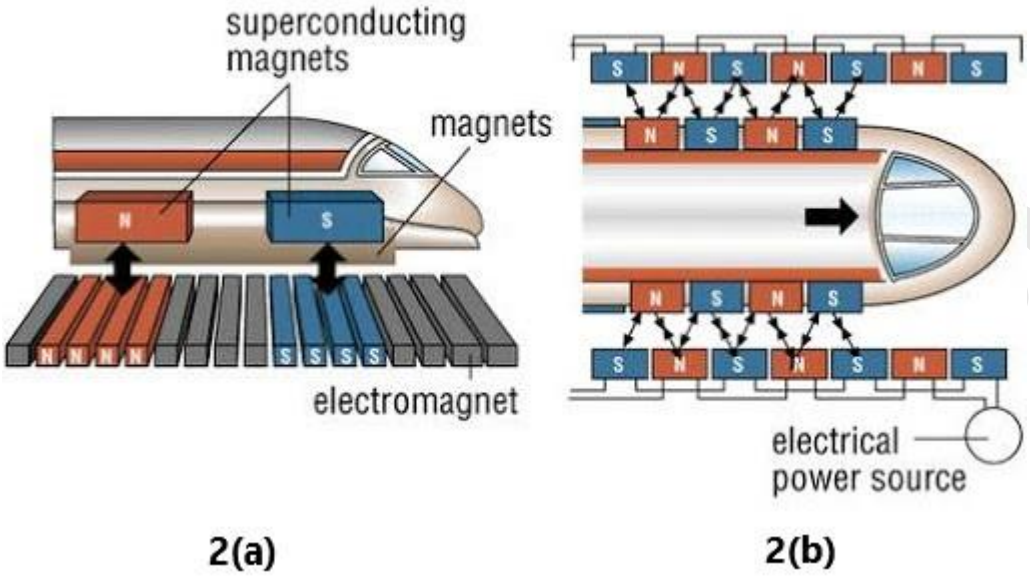

Figure 2(a) & 2(b). The working of Maglev Train which involves superconductor material and magnetic track (Resources from ffden-2.phys.uaf.edu website).

1.3 Problem statements

The problem statements for this project are:

1. YBCO thin film is time-dependent where the superconducting properties might decrease with the increasing of time which will affect the quality of the thin film.
2. The critical temperature of YBCO decreases continuously with increasing in oxygen deficiency thus reducing the superconductivity and quality of the YBCO thin film.

1.4 Objectives

The objectives of this project are:

1. To investigate the superconducting properties of YBCO thin film.
2. To observe the microstructure of YBCO thin film using X-ray diffraction, Atomic Force Microscopy and Scanning Electron Microscopy.

Chapter 2

LITERATURE REVIEW

2.1 History of Superconductor

Heike Kamerlingh Onnes, a Dutch physicist, discovered superconductivity when he successfully liquefied helium at 4.2 K while examining the resistivity of mercury. Timm, 2012 stated that in 1911, Onnes observed that the static resistivity of mercury suddenly dropped to zero at a critical temperature, T_c of about 4.1 K. Hence, the mercury at that critical temperature, T_c has entered a new state called the superconductive state due to the exceptional electrical properties. In December 1912, mercury was joined as a superconductor by tin and lead, metals with transition temperatures of 3.8 and 7.2 K, respectively. There was no need to experiment with delicate mercury capillaries after that (Van Delft & Kes, 2011).

The other crucial finding was that the magnetic field is expelled from a superconductor when the field is increased at temperature, T less than the critical temperature, T_c. With the magnetic field applied and the superconductor at low temperatures, the magnetic fields are still being prevented from penetrating the superconductors. This effect is now called the Meissner or Meissner-Ochsenfeld effect which is observed by W. Meissner and R. Ochsenfeld in 1933 (Timm, 2012). The Meissner effect is so powerful since a magnet

is able to levitate above a superconductive material where it causes this effect to also be referred as strong diamagnetism.

Three American physicists, John Bardeen, Leon Cooper, and John Schrieffer, proposed the first widely accepted theoretical explanation of superconductivity in 1957. Bardeen-Cooper-Schrieffer (BCS) theory of superconductivity is a theory that explains about Cooper pairs which usually exist in the low temperature superconductors. The BCS theory describes superconducting current as a superfluid of Cooper pairs, which are pairs of electrons that interact via phonon exchange (Arsenio et al., 2016). Owens & Poole, 2002 claimed that corresponding to a condition of zero resistance, the stability of a single state in which probability waves of electron pairs pass through a lattice without being scattered is predicted by BCS theory.

Yttrium barium copper oxide, $YBa_2Cu_3O_{7-x}$ (YBCO), is a ceramic compound that was discovered as a high temperature superconductor (HTS) in 1987 by Maw-Kuen Wu and Chu Ching-Wu. The discovery represents a major step forward in superconductivity since YBCO was the first material that exhibited superconductivity at the temperature of 92 K, which is above the boiling point of liquid nitrogen, 77 K at which typical chemical elements do not superconducts. In comparison to cuprate superconductors, such as YBCO, titanium diboride (TiB_2), and niobium pentoxide (Nb_2O_5), YBCO has a higher critical temperature of about 85 K for the same current density.

Before the discovery, there had been a surge of activity around the world aimed at studying the new superconductor's physics and identifying its potential applications. The discovery of YBCO's superconducting properties came into view from a purification process aimed at utilizing YBCO as an HTS material. This discovery was an important achievement

because instead of using the expensive liquid helium for cooling, liquid nitrogen could now be used.

Table 1. Chronology of superconductor discovery.

Year	Discovery
1911	H. Kamerlingh Onnes discovered superconductivity while experimenting with mercury.
1912	Onnes discovered that tin and lead also show superconductivity properties.
1933	W. Meissner and R. Ochsenfeld discovered Meissner effect.
1957	John Bardeen, Leon Cooper, and John Schrieffer proposed the Bardeen-Cooper-Schrieffer (BCS) theory of superconductivity.
1987	YBCO, a compound that shows superconductivity at a temperature above liquid nitrogen, was discovered by Maw-Kuen Wu and Chu Ching-Wu.

2.2 Superconductivity

Superconductivity occurs when electrical resistance in variety of solids completely disappears when they are cooled below critical temperature. When the electrical resistance of these materials entirely reaches zero value, the superconducting materials will repel each other. Onnes discovered these extraordinary properties when he first carried out an experiment on materials immersed in liquid helium in 1911 This experiment seems impossible to execute during that time. Figure 3 shows the first observation by Kamerlingh Onnes on mercury's resistance measurements, where it is clear that the resistance drops abruptly when it reaches the temperature of 4.2 K.

Although the material is kept considerably below critical temperature, T_c a high magnetic field above a specific critical value can cause a superconductor to revert to its non-superconducting phase, depending on the type of material.

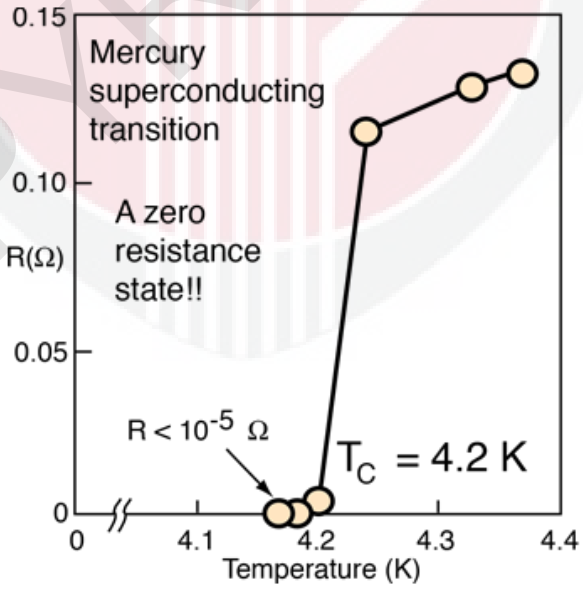

Figure 3. The resistance of mercury measured by Kamerlingh Onnes (H. K. Onnes, 1911).

2.3 Types of Superconductor

Superconductor exists in two types, which are Type I and Type II. Low Temperature Superconductors (LTC) or Type I, are usually made of pure metal. When cooled below its T_c, a Type I superconductor shows zero resistance and perfect diamagnetism. Apparently there is no magnetic field allowed inside a metal that is in superconducting state, where this phenomenon is known as the Meissner effect. (Owens & Poole, 2002). This indicates that Type I always have a complete Meissner effect. By having a low intensity of magnetic field, Type I superconductors can easily lose its superconducting state which is why Type I is also known as soft superconductors.

Type II or High Temperature superconductors (HTS) are hard superconductors since it does not easily lose its superconducting state. These superconductors are generally alloys and complex oxides of ceramics. Since an external magnetic field will be able to penetrate the surface of Type II superconductors to some extent, Type II is said to have an incomplete Meissner effect explaining why HTS is not completely diamagnetic. Additionally, HTS exhibits two critical magnetic field which can change states twice at two different magnetic field thresholds.

Figure 4 shows that Type I superconductors have a lower magnetic field compared to Type II. This means that Type II allows more penetration of the magnetic field into its surface while Type I expel the magnetic field from entering its surface.

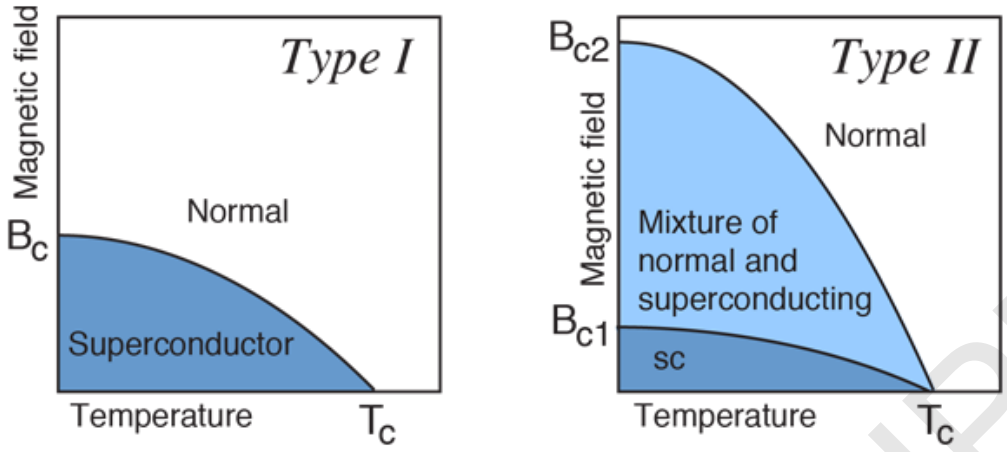

Figure 4. Type II superconductors have far higher critical magnetic fields than Type I superconductors, but they are combinations of normal and superconducting for the majority of that field range (Resources from hyperphysics.phy-astr.gsu.edu website).

2.4 Meissner Effects

A German professor W. Meissner and his doctoral student R. Ochsenfeld have discovered the Meissner effect in 1933 where this phenomenon is one of the essential properties of superconductivity. Meissner effect is a phenomenon of when a superconducting metal is cooled down below critical temperature while the magnetic field is applied to it which then the magnetic field will be expelled. This indicates that in a superconducting metal, magnetic field is not allowed in it. When a superconductor in a magnetic field is cooled to the point where it loses electrical resistance, the magnetic field within the material will be expelled (*Meissner Effect | Physics | Britannica*, n.d.). In contrast, when magnetic fields are applied to a normal metal, the fields completely flow through it.

The Meissner effect can be measured using both DC and AC magnetic fields in a variety of ways. In a magnetic field, the probe of a DC magnetometer, which detects magnetic field intensity, is placed close to the sample's surface. The field inside this sample is released as it cools below its superconducting critical temperature which then the magnetometer detects the corresponding increase in magnetic field strength outside the superconductor's surface.

Owens & Poole, 2002 described that an AC method can also be used to evaluate the Meissner effect. To achieve this, two small coils are twisted around the superconducting sample, an exciting inner coil and an outer probe coil then the latter is attached to a voltmeter. The current flow caused by an AC voltage provided to the exciting coil creates an AC magnetic field to flow across the sample. As a result, the voltmeter will detect an AC voltage in the probe coil. The AC magnetic field is then excluded from the sample when it is cooled below the critical temperature Tc, causing the AC field outside the sample to rise and increase the probe coil's voltage. As the probe voltage increases, the strength of the magnetic field ejected from the sample will increase too. Hence the magnitude of the Meissner effect can be measured.

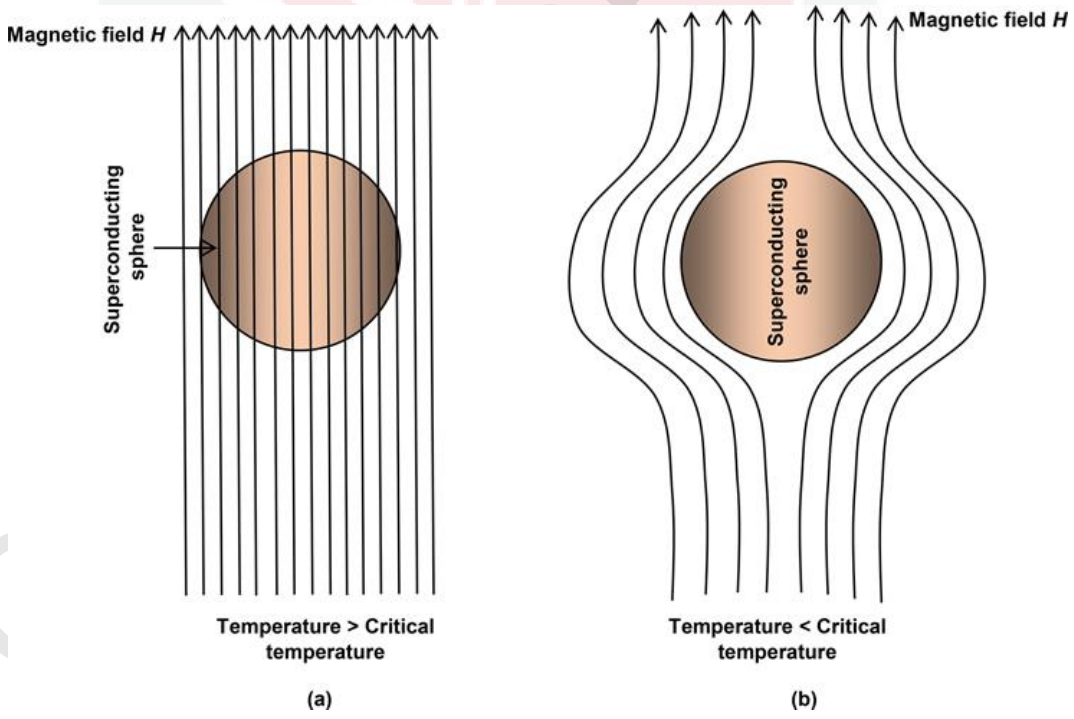

Figure 5(a) & 5(b). When a superconductor at temperature $T > T_c$ is placed in external magnetic fields, lines of magnetic field induction pass through its body but when it is cooled below the critical temperature $T < T_c$, the magnetic field lines are expelled out of the superconductor (Khanna, 2017).

2.5 Bardeen-Cooper-Schrieffer (BCS) Theory

BCS theory was developed in 1957 by American physicists, John Bardeen, Leon Cooper, and John Schrieffer to study the behavior of superconducting materials. This theory explains the phenomenon of when superconductors are cooled to temperatures near absolute zero, they lose all resistance to the flow of an electric current.

Cooper had discovered that electrons in a superconductor are gathered in pairs, which are now known as Cooper pairs, and that the motions of all Cooper pairs inside a single superconductor are correlated, forming a system that acts as a single organism. When voltage is applied to the superconductor, all cooper pairs will be in motion and act as a current. Even when the voltage is detached, the current will flow endlessly since there is no collision between the cooper pairs. The material will become non-superconducting when it is warmed up because the cooper pairs have separated into individual electrons.

The BCS theory also emphasizes many other characteristics of superconductor properties such as a critical field. This is the energy required to separate electrons in Copper pairs when a magnetic field is applied. (Owens & Poole, 2002). In addition, BCS theory also explains isotope effects. The temperature of the superconducting state is reduced when heavier atoms of the elements that make up the material are introduced.

2.6 Yttrium Barium Copper Oxide (YBCO) System

Yttrium Barium Copper Oxide (YBCO) is the first compound known to display superconductivity beyond the boiling point of liquid nitrogen (77 K), which was initially reported in 1987. This means that it was now possible to cool to these temperatures using liquid nitrogen.

Kumar, 2019 found that unlike the original simple metals and alloys, YBCO has highly complex crystal structures. The unit cell of $YBa_2Cu_3O_{7-x}$ is made up of three pseudocubic elementary perovskite unit cells. As shown in Figure 6, it has a Y or Ba atom in the centre, with Ba at the bottom of the unit cell, Y in the middle, and Ba at the top. Hence, along the c-axis, Y and Ba are stacked in the pattern [BaYBa]. Cu occupies all of the unit cell's corner sites and has two separate arrangements, Cu1 and Cu2 with respect to oxygen. As for oxygen, it has four possible crystallographic sites which are O_1, O_2, O_3 and O_4.

Hudner, 1993 proposed that depending on the value of x in the formula of YBCO, the structure can be either orthorhombic or tetragonal. The orthorhombic structure consists of CuO_2 planes intercalated by metal-oxygen layers. The basal planes of CuO perovskites are these CuO_2 planes, which are found in all HTS copper oxides. Every unit cell requires nine oxygen atoms to form a perfect perovskite structure. However, YBCO has only seven oxygen atoms which is why YBCO is often referred as an oxygen-deficient perovskite.

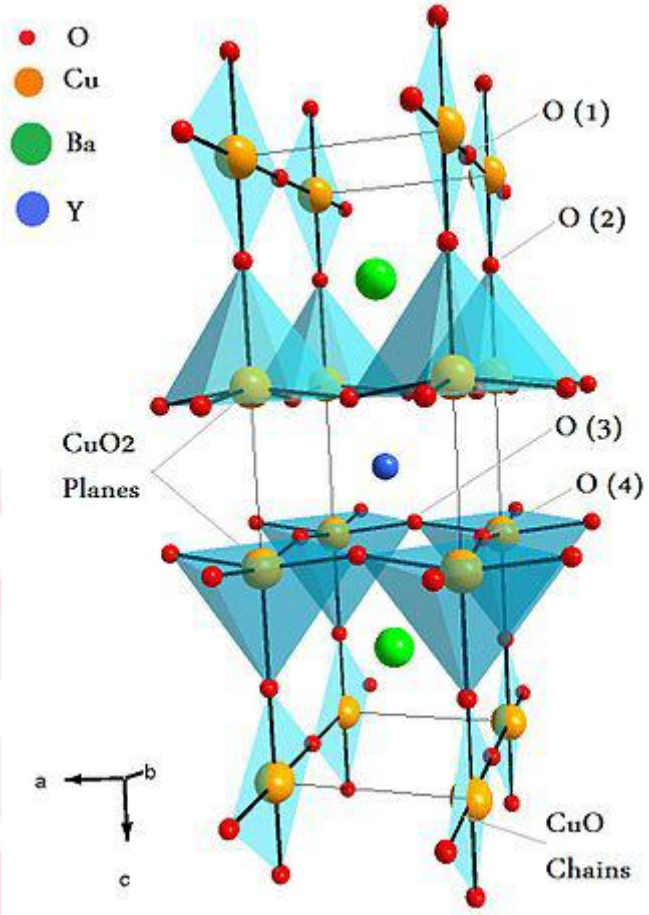

Figure 6. Crystal structure of YBCO where Y and Ba are stacked in the pattern [BaYBa] while Cu occupies all of the unit cell's corner sites with oxygen attached to it (Kumar, 2019).

2.7 Effect of Oxygen in Yttrium Barium Copper Oxide

Ever since the discovery of high temperature superconductors (HTS) including YBCO, the superconducting properties of this material are generally considered to be dependent on oxygen content. An increase in oxygen content increases the superconducting properties of YBCO and affect its crystal structure. YBCO is categorized as a perovskite structure where oxygen plays a significant role in determining if the material is either conductor or insulator.

The x-value in $YBa_2Cu_3O_{7-x}$ is a controlling factor for the material's structural and electrical properties where the increase of x will result in a rise of critical temperature, T_c. The YBCO structure gradually varies when x varies. As been mentioned by Benzi et al., 2004, an increase of oxygen content up from 6 to 6.5 (x = 1 – 0.5) makes it possible to obtain the tetragonal-semiconducting phase while for x = 0.5 the phase transition from tetragonal to orthorhombic occurs, over x = 0.2, the superconductive properties appear and for x = 0 the structure is completely orthorhombic-superconductive with T_c above 90 K.

When the range of the oxygen content is between 6.7~6.5, the T_c of YBCO remains constant but will also decrease if the oxygen content decreases continuously. The crystal structure of YBCO sample with 6.220 oxygen percent is orthorhombic, whereas the crystal structure of YBCO sample with 6.151 oxygen content is tetragonal (Suyama et al., 1991).

Many experimental methods have been used to evaluate the oxygen content in the high-T_c superconductors samples such as iodometric titration, coulometric titration, thermogravimetric analysis, micro-Raman spectroscopy, spectrophotometric method and volumetric method but all these measurements are destructive, so one knows the characteristics of the sample when it is no more useful (Benzi et al., 2004).

Chapter 3

METHODOLOGY

3.1 Introduction

This chapter will discuss more profound on the experimental setup used to complete this project which includes the sample characterization. This project aims to investigate the superconducting properties of YBCO thin film and observe the microstructure of YBCO thin film that was prepared by Pulsed Laser Deposition (PLD) method. Then, X-ray diffraction, Atomic Force Microscopy and Fields Emission Scanning Electron Microscopy are involved in this characterization. Figure 7 shows the flow chart of the method used to conduct this project.

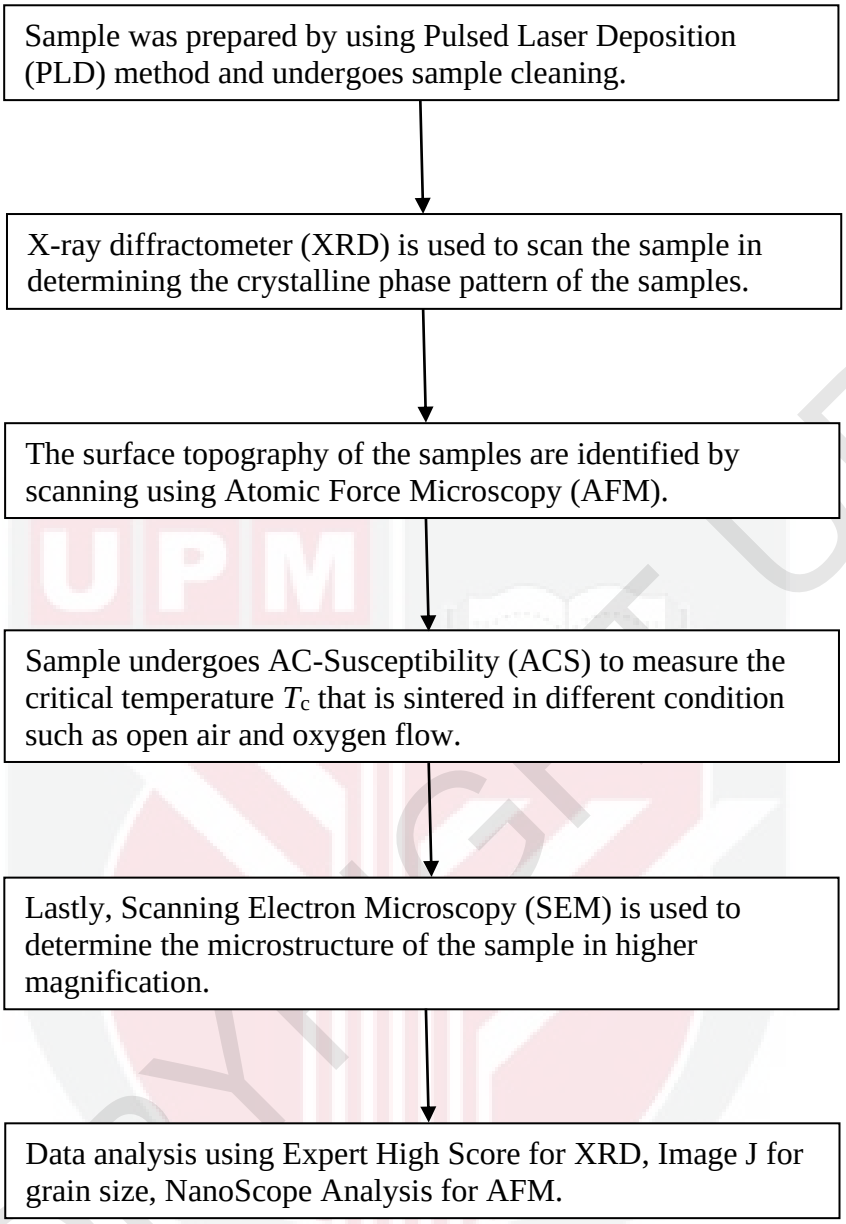

Figure 7. Flow chart on the overview procedure taken throughout this project.

3.2 Characterization

There are two properties of the YBCO samples to be observed which electrical and physical properties. A four-point probe is used to examine the electrical properties, while to characterize the physical properties, X-ray Diffraction (XRD) analysis, Atomic Force Microscopy (AFM), Scanning Electron Microscopy (SEM) and AC-Susceptometer (ACS) are used.

As for the physical properties, XRD is used to analyze the phase volume of the sample. Then, AFM and SEM are used to study the surface morphology of the YBCO sample. Lastly, to measure the critical temperature of the sample, ACS is used.

3.2.1 X-ray Diffraction (XRD)

X-ray Diffraction (XRD) is an analytical technique that functions to determine the crystallographic structure of a material. It is a method of irradiating a material with incident X-rays and then measuring the intensities and scattering angles of the X-rays that exit the material.

X-ray diffractometer comprises three elements which are X-ray tube, sample holder and X-ray detector. In order to produce an X-ray source for the system, the metal target is placed in the X-ray tube, where high energy and high voltage supplies are applied to the metal target. Following the generation of the X-ray, it is then filtered to produce monochromatic radiation that is more concentrated and directed towards the sample. The X-ray diffraction technique is used to investigate the crystal structure because the wavelength of X-ray radiation is relatively close to the interplanar spacing of most materials. The XRD technique is based on the principles of constructive interference.

When an electromagnetic wave is emitted from the crystal lattice, the intensity of peak was analysed at a certain conditions such as incident and scattered angle, polarization and wavelength. Bragg's law describes the relationship between the wavelength and the angle at which an x-ray diffracts. Bragg's law stated that when X-ray is scattered from the crystal lattice, the angle of the incident ray is equal to the angle of refracted ray. According to Bragg's law equation:

$$2d \sin \theta = n\lambda \qquad \text{Equation 1}$$

Where, d = inter planar spacing

θ = incident angle

n = the order of diffraction

λ = wavelength of X-ray.

When Bragg's law is fulfilled, the distance spacing between atomic planes and the crystalline structure can be obtained from the constructive interference of the diffracted X-ray beam. The intensity of peak refers to the position of particular atom lies in the structure and the total phases form in the sample. Hence, the crystal structure, lattice parameters and phase crystallinity of YBCO sample can be determined.

3.2.2 Atomic Force Microscopy (AFM)

Despite being a relatively new method, atomic force microscopy (AFM) has evolved into a powerful technology for characterizing the surface of materials down to the atomic scale (Khan et al., 2016). AFM is able to generate topographic surface maps with extremely high resolution and to view crystalline sample lattices at the atomic level.

AFM consists of the AFM probe as shown in Figure 8, which is a multi-cantilever with a very sharp tip that functions in surface sensing to scan over the surface of a sample. Due to the close-range, attractive force between the surface and the tip, the cantilever deflects towards the surface when the tip approaches it. The cantilever is able to scan the sample's surface in x, y and z directions perpendicular to the sample's surface.

However, as the cantilever is moved closer to the surface until the tip makes contact with the sample's surface, repulsive force takes over and the cantilever deflects away from the surface. This property can be applied to YBCO thin film since it uses the contact mode.

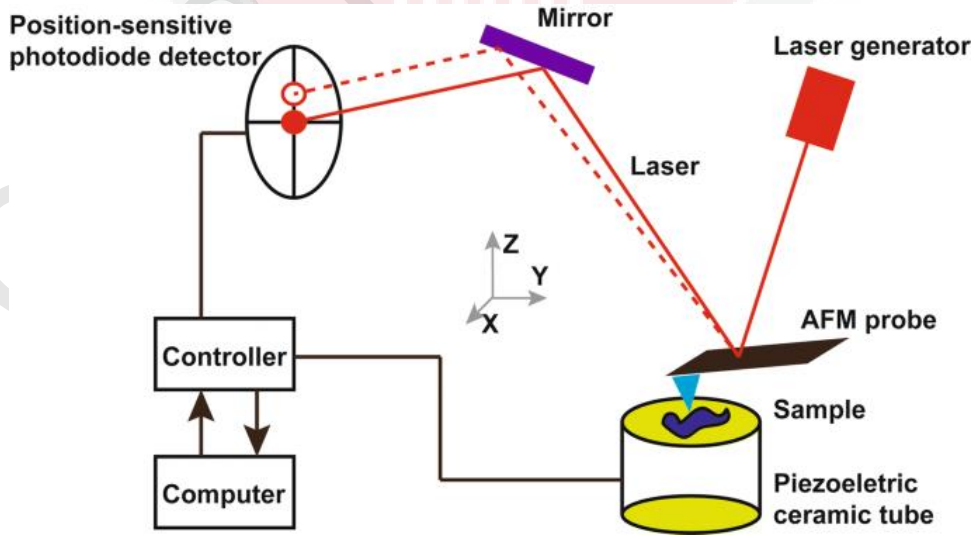

Figure 8. Schematic diagram of AFM working principle. AFM is composed of a piezoelectric ceramic tube, a laser generator, a position-sensitive photodiode detector, a

controller, and an AFM probe. The AFM probe is a micro-cantilever with a sharp tip attached at its end. (Deng et al., 2018).

A laser beam is used to detect cantilever deflections towards or away from the surface. By reflecting an incident beam off the flat top of the cantilever, any cantilever deflection will cause small variations in the direction of the reflected beam. A position-sensitive photo-diode (PSPD) can be utilized to track these changes. The PSPD records the cantilever deflection and consequent change in the direction of the reflected beam when an AFM tip passes over a raised surface feature. Analysis of these phase shifts as the cantilever scans over the surface is then used to form an image of the magnetic structure on the sample surface.

3.2.3 Scanning Electron Microscopy (SEM)

A Scanning Electron Microscopy (SEM) scans a beam of electrons over a specimen to produce a magnified image of an object. In this project, SEM is used to scan the morphology of particle size and shape, imperfection and topology of YBCO samples in nanometer size. When the electron beam reaches the surface, it penetrates the sample to a depth of a few microns, depending on the accelerating voltage and the density of the sample. Secondary electrons and x-rays are among the signals produced by this interaction inside the sample. Electrons are focused and deflected by electronic lenses to produce a narrow scan beam that moves in a zigzag pattern and thus bombard the sample.

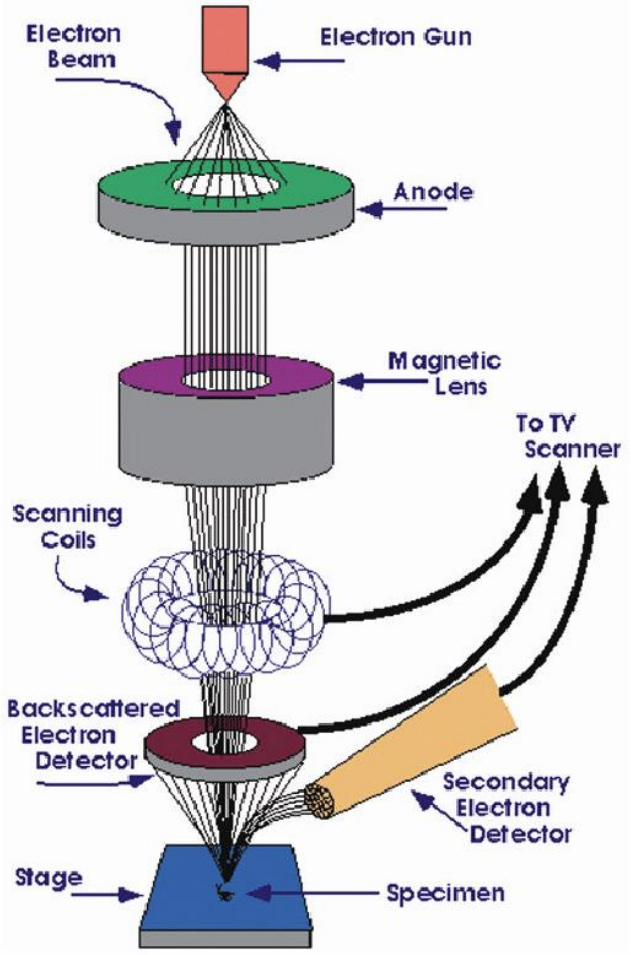

Figure 9. Schematic diagram of SEM (Joshi et al., 2008).

The highest resolution obtained in a SEM is determined by a number of criteria, including the size of the electron spot and the electron beam's interaction volume with the sample.

3.2.4 AC Susceptometer (ACS)

AC Susceptometer (ACS) is an important tool in sample characterization since it provides AC magnetic measurements. An AC field is applied to a sample that results in AC moment being measured. Since the induced sample moment is time-dependent, AC measurements provide information on the magnetization dynamic that is not available from DC measurements. The sample moment remains constant during the measurement period.

In AC magnetic measurements, a small AC driving magnetic field is overlaid on the DC field, resulting in a time-dependent moment in the sample. The time-dependent moment causes a current to flow through the pick-up coils, allowing measurement without moving the sample. The detecting circuitry is then set to exclusively detect in a small frequency band, which is generally the fundamental frequency.

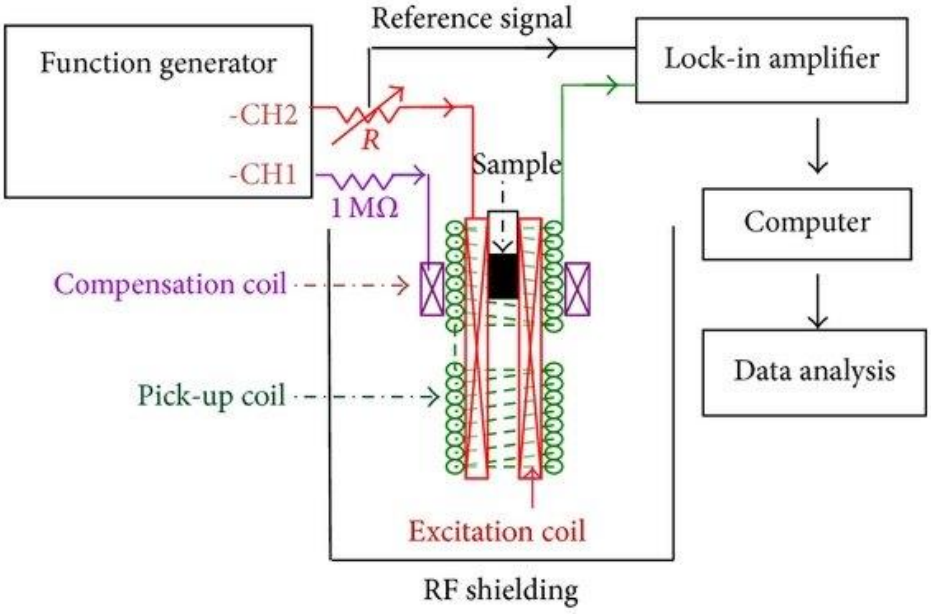

Figure 10. The detection scheme of an AC Susceptometer with a lock-in detection technique (Liao et al., 2015).

Chapter 4

RESULTS AND DISCUSSION

In this project, four types of characterization have been carried out to achieve the objectives of this project. The major focus of this project is to observe the samples' microstructure degradation such as the surface roughness and grain size using Atomic Force Microscopic (AFM). The topography of the samples has been observed by characterization using Scanning Electron Microscopy (SEM). The samples have been observed from magnification of 3000 until 5000 magnifications so that a higher-quality image of the samples can be obtained.

Table 2. List of thin films used for characterization.

Sample Code	Target	T_s(°C) Deposition Temperature	Deposition Oxygen pressure (mTorr)	Annealing Oxygen Pressure (Torr)
MUSTO11	$YBa_2Cu_3O_x$	780	400	726
MUSTO21	$YBa_2Cu_3O_x$	780	450	450
MYB05	$YBa_2Cu_3O_x$	780	450	450

4.1 Atomic Force Microscopic Analysis

Figure 11 until Figure 13 are different dimensions of AFM images of MUSTO11, MUSTO21 and MYB05 respectively. Figure 11 sequentially shows MUSTO11 at a) two dimension and b) three dimensions. As can be observe in the figure, MUSTO11 has the highest roughness which is 27.7 nm. This may due to the misorientation of the grains that clearly visible on Figure 11. Aghabagheri et al., 2016 reported that the high average roughness could be due to grain misorientation which this influence the surface roughness thus the oxygen pressure increased, the size of droplets and average roughness will increased too.

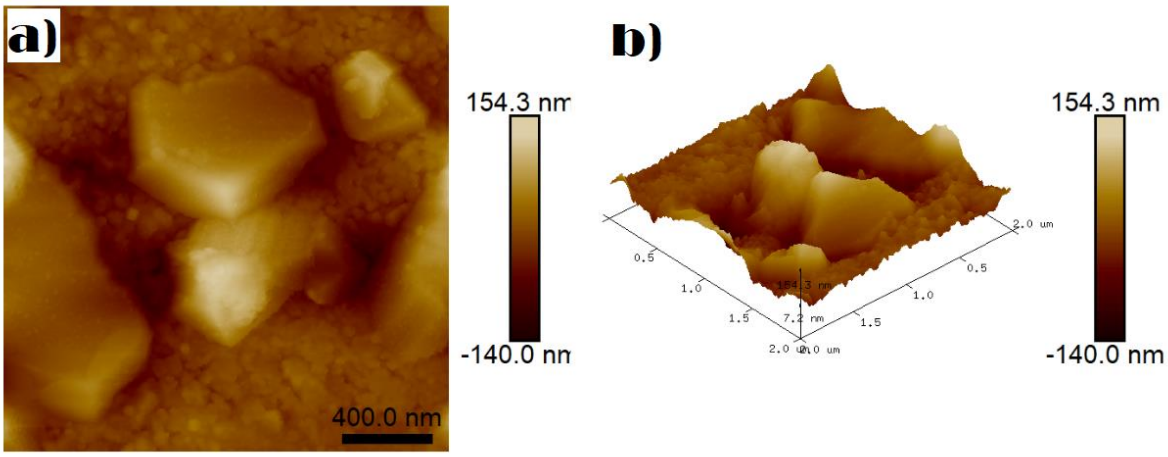

Figure 11. AFM images of MUSTO11 film at different. a) two dimension b) three dimension.

As for MUSTO21, the average surface roughness is 23.2 nm which is the smoothest surface morphology among the three films. It can be seen clearly in Figure 12 where the structures are closed to each other which indicates that the film is homogenous. Based on previous studies, homogeneity influences the superconducting properties of thin films. YBCO films with low surface roughness showed great quality epitaxial *c*-axis oriented growth with better superconducting properties (Xiong et al., 2013).

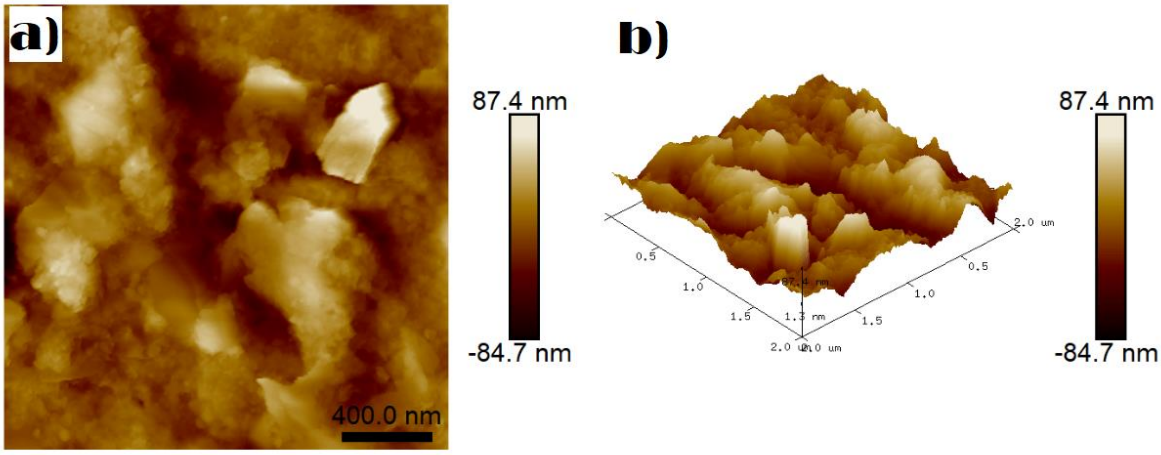

Figure 12. AFM images of MUSTO21 film at different dimension. a) two dimension b) three dimension.

Figure 13 shows the a) two dimension and b) three dimension of MYB05. The roughness of the sample's surface is 27.6 nm. It clearly visible on the figures that MYB05 shows more irregular-shaped grains compared to MUSTO11 and MUSTO21. There are more structures appear on this film. These structure are distributed randomly along the sample's surface. This indicates that the surface roughness of this sample is high.

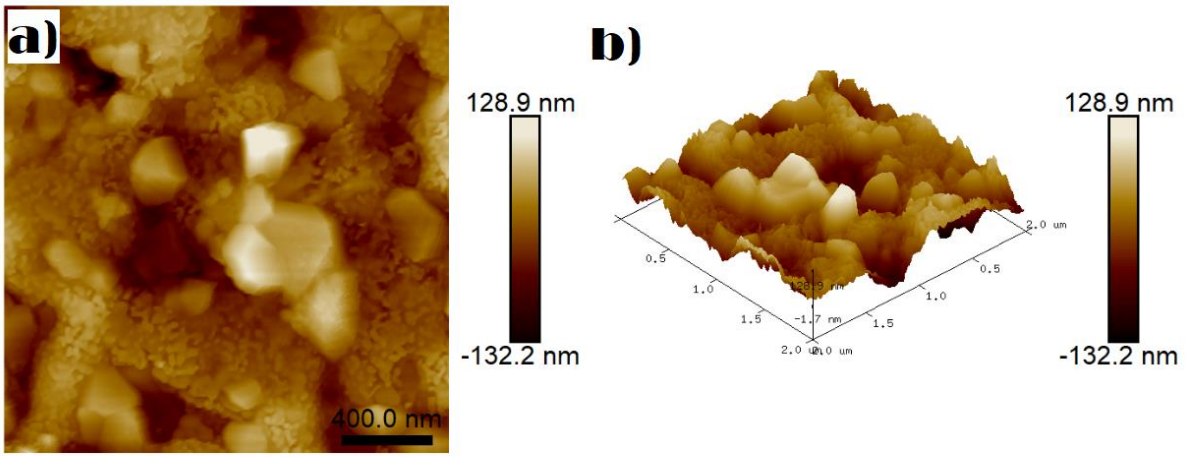

Figure 13. AFM images of MYB05 film at different dimension. a) two dimension b) three dimension.

Table 3. Average surface roughness of each thin films.

Sample	Average surface roughness (nm)
MUSTO11	27.7
MUSTO21	23.2
MYB05	27.6

4.2 Scanning Electron Microscopy (SEM) Analysis

Figure 14 to Figure 16 shown are the YBCO film's surface morphology which were examined by SEM. The images were captured under the magnification of 3000x, 5000x and 10 000x where these images can be enlarged.

Figure 14 shows the surface morphology area of MUSTO11 where a) 3000x magnification, b) 5000x magnification and c) 10000x magnification. The sample is composed of particulates with the average grain size of 1.980 μm. The grains have irregular shape that is distributed randomly and have variants of crystallinity along the sample surface. MUSTO11 has the biggest grain size compared to other films.

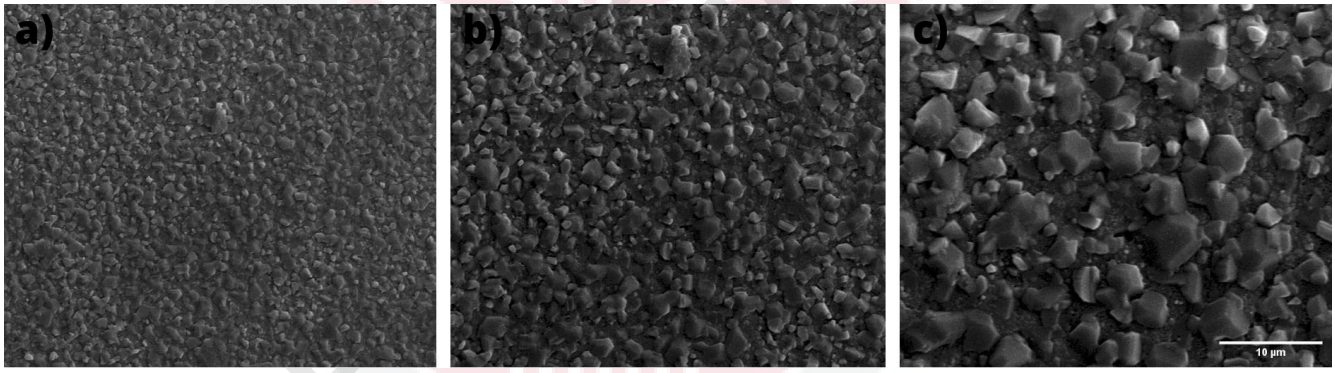

Figure 14. SEM images of MUSTO11 under magnification of a) 3000x b) 5000x c) 10000x.

The SEM images of MUSTO21 are shown in Figure 15 where it shows in a) 3000x b) 5000x and c) 10000x magnifications. It can be seen clearly that there are small amount of porosity appeared in the sample. The resistivity of the sample has decreased while the J_c value has increased due to the presence of porosity (Senawi et al., 2015). MUSTO21 has the smallest grain size which is 1.076 μm. The small grain size surely affects the

superconductivity of the film because according to Yang et al., 2002 the levitation force reduces as grain size decreases.

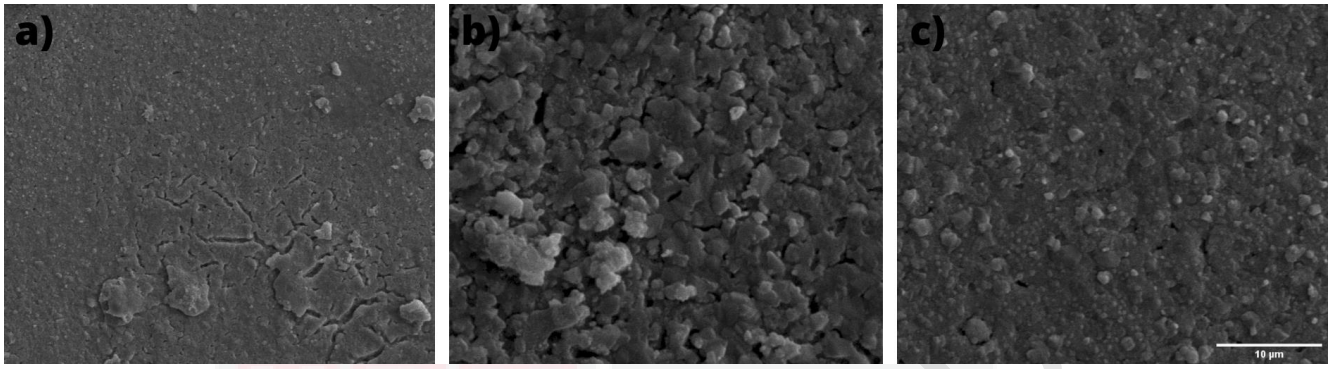

Figure 15. SEM images of MUSTO21 under magnification of a) 3000x b) 5000x c) 10000x.

Figure 16 reveals the SEM images of MYB05. The grains are clearly visible in irregular shapes and are far apart from each other. The average grain size for this sample is 1.704 µm. There are existance of holes which can be seen on the images.

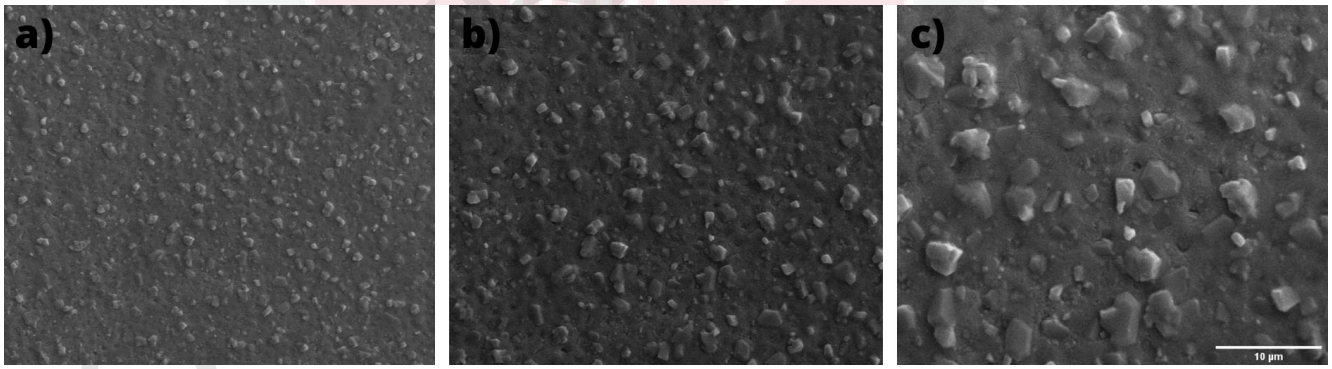

Figure 16. SEM images of MYB05 under magnification of a) 3000x b) 5000x c) 10000x.

Table 4. Average grain size of each films.

Sample	Average Grain Size
MUSTO11	1.980 ± 0.859 µm
MUSTO21	1.076 ± 0.649 µm
MYB05	1.704 ± 0.881 µm

4.3 Elemental Analysis via Energy Dispersion X-ray

Energy Dispersive Spectroscopy (EDS) analysis was performed on all samples in order to determine the Y: Ba: Cu: O composition ratio. Figure 17 to 19 display the results of the EDX analysis. Tables 5 to 7 provide the atomic percentages of the elements in each spectrum.

Figure 17 reveals the elements exists in the samples as tabulated in Table 5. The ratio of Y: Ba: Cu for spectrum 2 is 4.55:10.74:17.05 which is the nearest to Y123 composition compared to other samples. Although Copper has higher average atomic percentage, Barium is the dominant element since it has the highest average weight percentage.

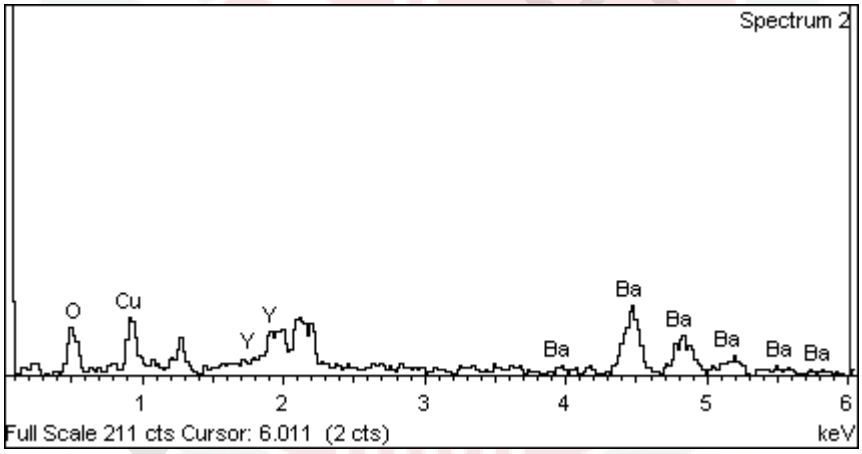

Figure 17. EDX surface analysis of MUSTO11.

Table 5. Quantitative elemental analysis of MUSTO11 film obtained by EDS analysis.

Element	Shell	Weight %	Atomic %
O	K	26.75	67.66
Cu	L	26.78	17.25
Y	L	10.01	4.55

Ba	L	36.46	10.74

The average atomic percentage for MUSTO21 is tabulated in Table 6 where the ratio is 6.21:10.37:18.11 for Y:Ba:Cu respectively. This sample's composition is near Y123 composition.

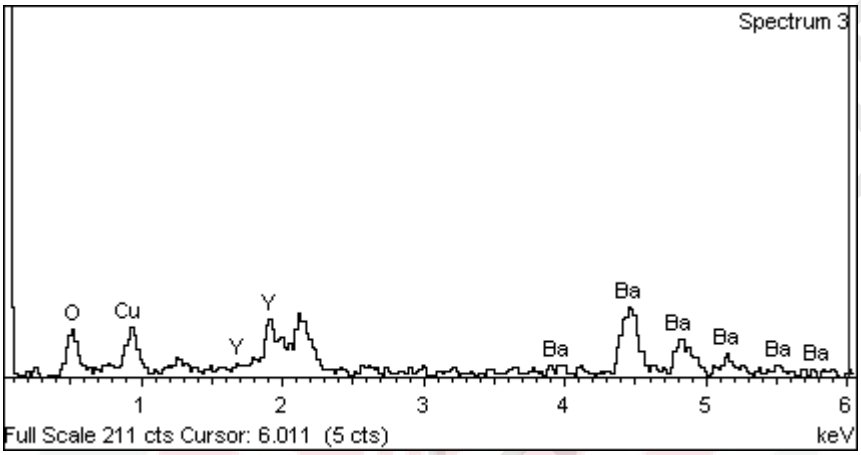

Figure 18. EDX surface analysis of MUSTO21.

Table 6. Quantitative elemental analysis of MUSTO21 film obtained by EDS analysis.

Element	Shell	Weight %	Atomic %
O	K	25.05	65.31
Cu	L	27.58	18.11
Y	L	13.23	6.21
Ba	L	34.14	10.37

Table 7 shows that spectrum 3 has near Y123 composition. The result obtained by calculating the average atomic percentage for spectrum 3 is 10.23:17.75:23.61 for Y:Ba:Cu respectively. Barium is the dominant element since the average weight percentage is the highest although Copper has higher average atomic percentage.

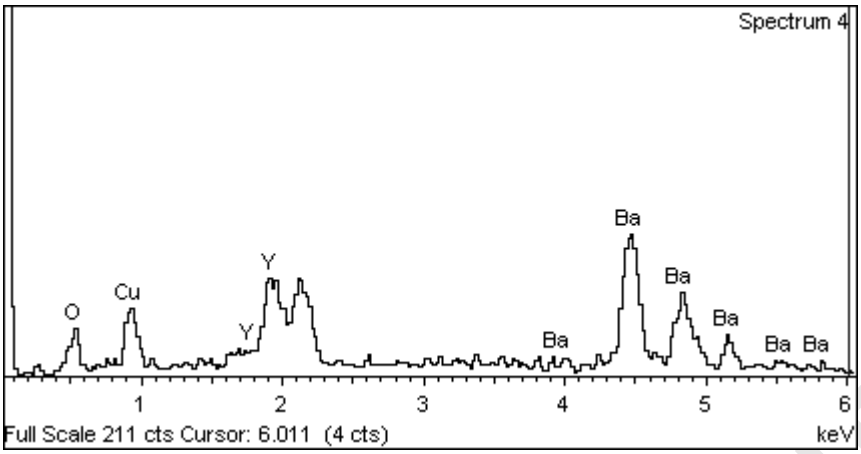

Figure 19. EDX surface analysis for MYB05.

Table 7. Quantitative elemental analysis of MYB05 film obtained by EDS analysis.

Element	Shell	Weight %	Atomic %
O	K	13.78	48.41
Cu	L	26.69	23.61
Y	L	16.17	10.23
Ba	L	43.96	17.75

4.4 X-ray Diffraction (XRD) Analysis

In order to validate the presence of superconducting phases, X-ray diffraction analysis was performed on the all of the YBCO samples. The samples were scan at the range of 20-80 degrees (2^{o}Theta) and the diffraction pattern for each samples were indexed by comparing with the diffraction patterns. The data were analysed using X'pert Highscore Plus Software.

However, there are no peaks present on all three samples. This may due to the size of the samples are too small which causes the x-ray to unable to penetrate through them. Other than that, the films might also lose their crystallinity over time since the films were deposited on 2007 which is 15 years ago. During this period, the film may had exposure to the surrounding where surface degradation might occur. Surface deterioration of YBCO is common when exposed to the environment (Du et al., 2001). Eventhough proper steps were taken to store the YBCO thin film such as by storing the samples in a dry N_2 cabinet which supposedly able to minimize the rate of reaction on the film, surface degradation might still occur since it was stored for 15 years. This surely proves that YBCO thin film is time-dependent where the superconductivity will decrease with the increasing of time. In addition, the orthorhombicity of the films might also decrease due to decreasing oxygen content. The samples were unable to undergo another test run due to some issues.

Chapter 5

CONCLUSION

5.1 Conclusion

Characterization of YBCO thin film by analysis such as AFM analysis, SEM analysis, EDX analysis and XRD analysis has been done throughout this project. The microstructure, surface morphology, element composition, phase structure and superconducting properties of the thin films has been studied accordingly.

X-ray diffraction has been carried out in order to investigate the phase formation of $YBa_2Cu_3O_{7-x}$ films. Unfortunately, no phase formation or YBCO peaks were obtained after the analysis due to the size of the sample is too small and also due to unavoidable circumstances.

Atomic force microscopy and scanning electron microscopy were also carried out to study the surface morphology and topology of the samples where the average surface roughness and average grain size of each samples varies. The average surface roughness increased due to increased in oxygen pressure. The average grain size may affect the superconducting properties of YBCO thin film such as the levitation will reduce as the grain size decrease.

5.2 Reccomendation and suggestion

Based on the theoretical and experimental results obtained in this project, further research regarding the following fields are recommended:

i. How environmental exposure may affects the thin film.

ii. The thin film is time-dependent, hence other treatments such as post-annealing treatment should be done in order to improve the structure and superconducting properties of the film.

References

Aghabagheri, S., Mohammadizadeh, M. R., Kameli, P., & Salamati, H. (2016). Effect of Oxygen Pressure on the Surface Roughness and Intergranular Behavior of YBCO Thin Films. *Journal of Superconductivity and Novel Magnetism*, *29*(6), 1483–1489. https://doi.org/10.1007/s10948-016-3457-7

Arsenio, A. J., Carvalho, M. V., Cardeira, C., Branco, P. J. C., & Melicio, R. (2016). Viability of a frictionless bearing with permanent magnets and HTS bulks. *Proceedings - 2016 IEEE International Power Electronics and Motion Control Conference, PEMC 2016*, 1231–1236. https://doi.org/10.1109/EPEPEMC.2016.7752172

Benzi, P., Bottizzo, E., & Rizzi, N. (2004). Oxygen determination from cell dimensions in YBCO superconductors. *Journal of Crystal Growth*, *269*(2–4), 625–629. https://doi.org/10.1016/j.jcrysgro.2004.05.082

Deng, X., Xiong, F., Li, X., Xiang, B., Li, Z., Wu, X., Guo, C., Li, X., Li, Y., Li, G., Xiong, W., & Zeng, Z. (2018). Application of atomic force microscopy in cancer research. In *Journal of Nanobiotechnology*. BioMed Central Ltd. https://doi.org/10.1186/s12951-018-0428-0

Du, J., Lam, S. K. H., & Tilbrook, D. L. (2001). Metallization and interconnection of HTS YBCO thin film devices and circuits. *Superconductor Science and Technology*, *14*(10), 820–825. https://doi.org/10.1088/0953-2048/14/10/303

Hudner, J. (1993). *Superconducting thin films of Royal Institute of Technology, Department of Solid Sute Electronics (1993) (TRITA-FTE-Research report 1993:3) ABSTRACT*.

Joshi, M., Bhattacharyya, A., & Ali, S. W. (2008). Characterization techniques for nanotechnology applications in textiles. *Indian Journal of Fibre and Textile Research*, *33*(3), 304–317.

Khan, M. K., Wang, Q. Y., & Fitzpatrick, M. E. (2016). Atomic Force Microscopy (AFM) for Materials Characterization. In *Materials Characterization Using Nondestructive Evaluation (NDE) Methods* (pp. 1–16). Elsevier Inc. https://doi.org/10.1016/B978-0-08-100040-3.00001-8

Khanna, V. K. (2017). Superconductive electronics for ultra-cool environments. In *Extreme-Temperature and Harsh-Environment Electronics Physics, technology and applications*. IOP Publishing. https://doi.org/10.1088/978-0-7503-1155-7ch12

Kumar, S. (2019). *High Temperature Superconductors : An Overview High Temperature Superconductors : An Overview*. https://doi.org/10.13140/RG.2.2.32727.21921

Lee, H. W., Kim, K. C., & Lee, J. (2006). Review of Maglev train technologies. In *IEEE Transactions on Magnetics*. https://doi.org/10.1109/TMAG.2006.875842

Liao, S. H., Chen, J. H., Su, Y. K., Chen, K. L., Horng, H. E., & Yang, H. C. (2015). Assaying biomarkers via real-time measurements of the effective relaxation time of biofunctionalized magnetic nanoparticles associated with biotargets. *Journal of Nanomaterials*. https://doi.org/10.1155/2015/497296

Meissner effect | physics | Britannica. Retrieved June 4, 2021, from https://www.britannica.com/science/Meissner-effect

Owens, F. J., & Poole, C. P. J. (2002). The New Superconductors. *Journal of Chemical Information and Modeling*, *53*(9), 1689–1699.

Senawi, S. A., Azhan, H., Zainal, W. N. F. W., Razali, W. A. W., Nazree, A., Azman, K., Ridzwan, H. J. M., Norazidah, A. W., Hidayah, H. N., & Hawa, J. S. (2015). Porosity Effect on Superconducting Properties of $YBa_2Cu_3O_\delta$ and $YCaBa_4Cu_6O_\delta$. *Advanced Materials Research*, *1107*, 601–605. https://doi.org/10.4028/www.scientific.net/amr.1107.601

Sharma, R. G. (2015). Other applications of superconducting magnets. *Springer Series in Materials Science*, *214*, 359–404. https://doi.org/10.1007/978-3-319-13713-1_10

Suyama, Y., Matsumoto, M., Kageyama, S., & Sato, I. (1991). Effect of Oxygen Deficiency on the Superconducting Properties of YBCO. In *Advances in Superconductivity III* (pp. 391–394). Springer Japan. https://doi.org/10.1007/978-4-431-68141-0_86

Timm, C. (2012). *Theory of Superconductivity. Institute of theoretical Physics Dresden.*

Urone, P. P., & Hinrichs, R. (2012). *Magnetic Field Strength: Force on a Moving Charge in a Magnetic Field*. OpenStax.

Van Delft, D., & Kes, P. (2011). The discovery of superconductivity. *Europhysics News*, *42*(1), 21–25. https://doi.org/10.1051/epn/2011104

Velavan, R., & Myvizhi, P. (2018). Superconductors and its Applications 1. *International Journal of Pure and Applied Mathematics*, *119*(12), 7377–7386.

Xiong, J., Xia, Y., Zhang, F., Xue, Y., Hu, K., Zhao, X., & Tao, B. (2013). The influence of surface morphology of buffer layer on the critical current density in YBCO coated conductors. *Advances in Condensed Matter Physics*. https://doi.org/10.1155/2013/673948

Yaghoubi, H. (2013). The most important maglev applications. In *Journal of Engineering (United Kingdom)*. Hindawi Limited. https://doi.org/10.1155/2013/537986

Yang, W. M., Zhou, L., Feng, Y., Zhang, P. X., Zhang, C. P., Yu, Z. M., Tang, X. D., Nicolsky, R., & Andrade, R. (2002). Identification of the effect of grain size on levitation force of well-textured YBCO bulk superconductors. *Cryogenics*, *42*(10), 589–592. https://doi.org/10.1016/S0011-2275(02)00075-9